Guo *et al.*
Chinese Journal of Mechanical Engineering (2022) 35:84
https://doi.org/10.1186/s10033-022-00764-7

Chinese Journal of Mechanical Engineering

ORIGINAL ARTICLE

Open Access

Morphological Heredity of Intermetallic Nb_5Si_3 Dendrites in Hypereutectic Nb-Si Based Alloys via Non-Equilibrium Solidification

Yueling Guo[1*], Lina Jia[2*], Wenjun Lu[3] and Hu Zhang[2]

Abstract

For hypereutectic Nb-Si based alloys, primary Nb_5Si_3 phases typically grow in a faceted mode during equilibrium or near-equilibrium solidification, which damages the ductility and toughness. To address this issue, here we artificially manipulate the growth morphology of Nb_5Si_3 using electron beam surface melting (EBSM) and subsequent annealing treatments. Results show that such a non-equilibrium solidification pathway enables the transition from faceted growth to non-faceted dendritic growth of Nb_5Si_3, along with evident microstructure refinement, generation of metastable β-Nb_5Si_3 phases and elimination of chemical segregation. The transformation from β-Nb_5Si_3 to α-Nb_5Si_3 and Nb solid solution (Nbss) particles is triggered by the annealing treatment at 1450 °C for 5 h. Also, we find the annealing-mediated formation of inherited Nb_5Si_3 dendrites that maintain the dendritic morphology of the original as-solidified β-Nb_5Si_3 dendrites. This work thus provides a feasible routine to obtain thermally stable and refined α-Nb_5Si_3 dendrites in hypereutectic Nb-Si based alloys.

Keywords: Nb-Si alloy, Intermetallics, Nb_5Si_3, Rapid solidification, Dendritic growth

1 Introduction

For increased efficiency and performance of advanced turbine engines, there is always a driving force to increase the inlet temperature [1]. This demand motivates the design and production of novel ultrahigh temperature materials (UHTM) that can operate at higher temperatures than current Ni-based superalloys [1, 2]. As a member of UHTM family, Nb-Si based alloys, consisting of Nb solid solution (Nbss) and silicides (mainly Nb_5Si_3), have been of interest due to their high melting temperatures (> 1750 °C), relatively low densities (< 7.2 g/cm^3) as well as excellent creep resistance with creep rates below 3×10^{-8} s^{-1} at 1200 °C and stresses above 140 MPa [1, 3, 4].

The introduction of intermetallic Nb_5Si_3 contributes largely to such property advantages, as a density reducer and a high temperature strength enhancer. But unfortunately, Nb_5Si_3 normally causes the loss of ductility and toughness at room temperature, acting as the preferred sites for crack initiation and propagation, especially for hypereutectic Nb-Si based alloys [5, 6]. Tuning the geometrical morphology and length scale of Nb_5Si_3 can be an effective pathway to achieve better alloy property, provided that its growth behavior is well understood and suited solidification processing techniques are employed [6, 7].

In conventional cast Nb-Si based alloys, Nb_5Si_3 particles are normally distinguished by a faceted growth morphology [7–9], because of its high entropy of fusion and large Jackson's factor (α) of ~2.2 [10]. It thus suggests the growth of Nb_5Si_3 is typically limited by the nucleation rate under slow-cooling and near-equilibrium solidification conditions. Recent experimental evidences demonstrates that wide microstructural variations can be

*Correspondence: y.guo@bit.edu.cn; jialina@buaa.edu.cn

[1] School of Mechanical Engineering, Beijing Institute of Technology, Beijing 100081, China
[2] Research Center of Light-alloy Materials, Frontier Institute of Science and Technology Innovation, Beihang University, Beijing 100191, China
Full list of author information is available at the end of the article

achieved via rapid solidification, including morphology, phase size and volume fraction [11–13].

For rapidly solidified alloys, the growth mode of thermodynamics-controlled faceted phases, may be altered concomitantly, e.g., the transition from faceted to non-faceted growth of intermetallic phases with high entropy of fusion [14, 15]. The mechanism behind this morphology transition is mainly due to the change in the solid/liquid interface structures and roughness [16, 17]. Previous literature [6, 12, 18] has reported that beneficial microstructure modification of Nb-Si based alloys is enabled by rapid solidification, resulting in improvements of oxidation resistance and fracture toughness. The non-faceted growth of Nb_5Si_3 dendrites has been observed as result of non-equilibrium solidification [12, 19], but the corresponding growth mechanism still lacks. More importantly, the thermal and morphological stabilities of Nb_5Si_3 formed via rapid solidification remains unexplored yet, which is of particular importance for Nb-Si based alloys with potential high temperature applications.

In this work, we shift our research focus on the phase stability and morphology of Nb_5Si_3 upon rapid solidification and high temperature exposure. Nb_5Si_3 dendrites are produced via electron beam surface melting (EBSM, a direct liquid/solid solidification approach) and via subsequent annealing treatment (an inherited solid/solid phase transformation approach). The morphological heredity of intermetallic Nb_5Si_3 dendrites found here can offer a novel insight into the control of silicide morphology in Nb-Si based alloys. Note that the solidification condition of EBSM is similar to the state-of-the-art technique of additive manufacturing [20], and therefore, this work is considered as a suitability pre-evaluation of Nb-Si based alloys for electron beam additive manufacturing, and a guidance for microstructure design towards mechanical property improvement.

2 Materials and Methods

The Nb-22Si-24Ti-2Cr-2Al (at.%) alloys were employed in this work, fabricated by non-consumable arc-melting using high-purity staring materials of Nb (99.87 wt.%), Si (99.50 wt.%), Ti (99.76 wt.%), Cr (99.98 wt.%) and Al (99.99 wt.%). The button ingots were remelted by vacuum induction melting (VIM), in order to improve chemical homogeneity. Mechanically ground alloy disks were prepared for EBSM treatment, which was carried out using an Arcam A2XX (Arcam AB) electron beam 3D printing system with a controlled 0.2 Pa of He atmosphere. The electron beam was generated in an electron gun via a tungsten filament, which was heated to above 2000 °C. The emitted electrons were accelerated by an electrical field and focused by an electromagnetic coil. Controlled by a computer attached to the 3D printing system, the focused electron beam was selectively scanned on the Nb-Si based alloy substrate. For cracking prevention, the substrate was preheated to 1200 °C by defocused electron beam before scanning. A processing current of 4.2 mA and the zigzag scanning strategy with a scanning speed of 170 mm/s were employed. The hatch distance was 0.1 mm. Annealing treatment was performed at 1450 °C for 5 h to examine the microstructural stability, and the samples were sealed in silica tubes to avoid oxidation. Furnace cooling was utilized in this work, with an average cooling rate of approximately 10 °C/min.

Phases were determined by X-ray diffraction (XRD, D/max-2500, Cu *K*α) with a 2θ scanning rate of 6°/min. Backscattered electron (BSE) imaging was performed using a scanning electron microscopy (SEM, Zeiss-Merlin) with an acceleration voltage 30 kV. The elemental distributions measured using the attached energy-dispersive X-ray spectroscopy (EDS). Electron backscatter diffraction (EBSD) was performed using a Zeiss-Crossbeam XB 1540 FIB instrument with a Hikari camera operating at 15 kV. The EBSD scanning step sizes for the VIM and EBSM alloy were 1 μm and 0.1 μm, respectively. A TSL OIM package was used for data collection and analysis.

Microstructure of the annealed alloy was imaged by a scanning transmission electron microscopy (STEM, image-corrected FEI Titan Themis 80-300) with the high-angle annular dark-field (HAADF) imaging mode. The acceleration voltage for HAADF-STEM imaging was 300 kV. For HAADF-STEM imaging, a probe semi-convergence angle of 17 mrad and inner and outer semi-collection angles ranging from 73 to 200 mrad were conducted. Selected area diffraction (SAD) was performed on a JEOL JEM 2100 instrument for phase identification. The simulated SAD patterns were obtained by CaRIne v3.1 software. The thin lamellae for TEM investigation, ~10 μm in width, were extracted from the Nb_5Si_3 silicide within the annealed EBSM alloy using a dual-beam focused ion beam (FIB)/SEM instrument (FEI Helios Nanolab 600i). The standard site-specific lift-out procedure was applied for FIB-thinned lamellae [21]. The FIB-induced damage and Ga ions contamination were minimized by a final cleaning at 5 kV.

3 Results

According to the XRD patterns shown in Figure 1, the original VIM alloy is mainly composed of bcc-structured Nbss and tetragonal α-Nb_5Si_3 with a $D8_1$ structure, and the experimental EBSM alloy primarily consists of Nbss and tetragonal β-Nb_5Si_3 with a $D8_m$ structure. After annealing treatment at 1450 °C for 5 h, the main phases of the EBSM include Nbss, α-Nb_5Si_3 and β-Nb_5Si_3. Depending on alloy compositions and processing methods, three polymorphs of Nb_5Si_3 have been reported, i.e., α-Nb_5Si_3

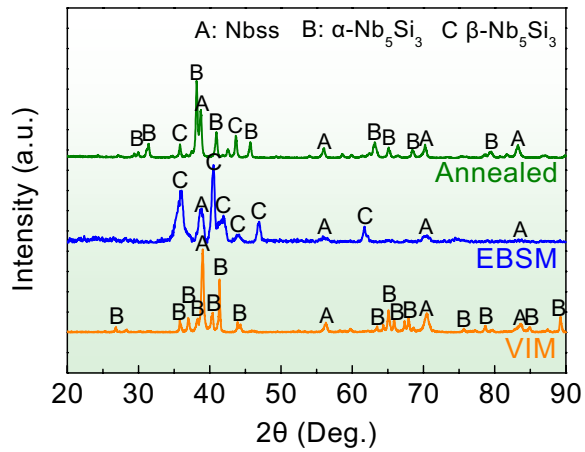

Figure 1 XRD patterns of the hypereutectic Nb-Si based alloys processed by VIM and EBSM

($tI32$, $D8_l$), β-Nb_5Si_3 ($tI32$, $D8_m$) and γ-Nb_5Si_3 ($hP16$, $D8_8$) [22]. This work suggests that the rapid solidification process induced by EBSM leads to the formation of β-Nb_5Si_3, but the subsequent annealing treatment promotes the transition from β-Nb_5Si_3 to α-Nb_5Si_3 that is more stable at lower temperatures [23].

Figure 2(a) displays the BSE image of the VIM alloy, and the EBSD phase map is shown in Figure 2(b). The VIM alloy without remelting shows a hypereutectic microstructure, and the primary faceted α-Nb_5Si_3 particles (dark grey contrast) are observed, in combination with Nbss phases (light grey contrast). It is observed that α-Nb_5Si_3 particles are embedded in the Nbss matrix. α-Nb_5Si_3 shows a faceted polygonal morphology with a coarse size up to ~80 μm. According to EDS line scanning (Figure 2(c)) and EDS mapping (Figure 2(d)), α-Nb_5Si_3 is enriched in Si, but depleted in Nb, Ti, Cr and Al, compared with Nbss. The black contrast region, mainly on the edge of α-Nb_5Si_3, contains a higher content of Ti. Within Nbss matrix, the chemical segregations of Ti and Cr are noted.

Figure 3 shows the sectional microstructure of the experimental alloy subjected to EBSM treatment, and a remelted layer, ~188 μm in thickness, is produced on the surface. The remelted layer is typically generated by the overlap of molten pools, which is essentially identical to the welding and additive manufacturing processes [24, 25]. Molten pool boundary is defined as the partitioning line between adjacent molten pools. The microstructure beneath the remelted layer is identical to that of the VIM alloy, suggesting no additional effect is caused by the EBSM treatment. It is evident that compared to the VIM alloy, the remelted layer demonstrates a significantly finer microstructure.

For the remelted layer via EBSM, the microstructure within molten pool is shown in Figure 4(a) and (b). In combination with the XRD result in Figure 1, the dark-grey phase should be β-Nb_5Si_3, and the light-grey phase is Nbss. β-Nb_5Si_3 dendrites are directly formed upon the solidification process of EBSM, with a composition of 50.16Nb-28.66Si-18.48Ti-0.59Cr-2.10Al (at.%), as measured by SEM-EDS. Nanoscale silicide particles are observed among β-Nb_5Si_3 dendrites. According to the

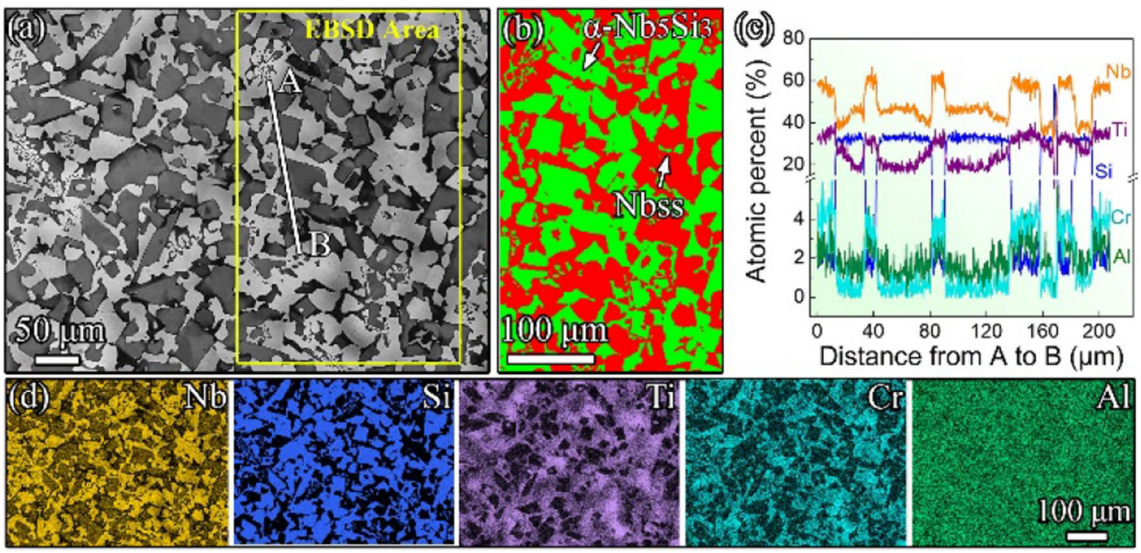

Figure 2 Microstructures and elemental distributions of the hypereutectic Nb-Si based alloy via VIM: (**a**) BSE image; (**b**) EBSD phase map; (**c**) EDS scanning along line AB plotted in (**a**); (**d**) EDS mappings of (**a**)

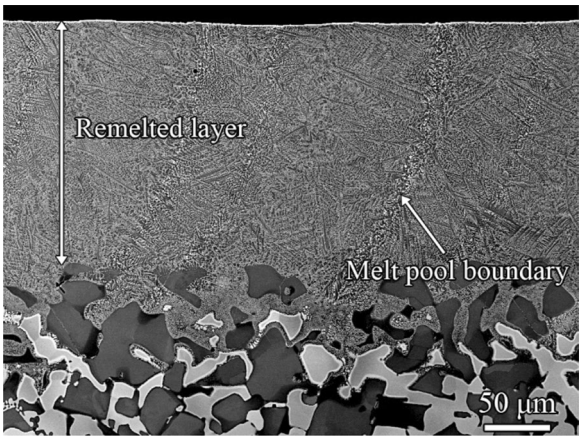

Figure 3 BSE image of the remelted layer produced on the hypereutectic Nb-Si based alloy via EBSM

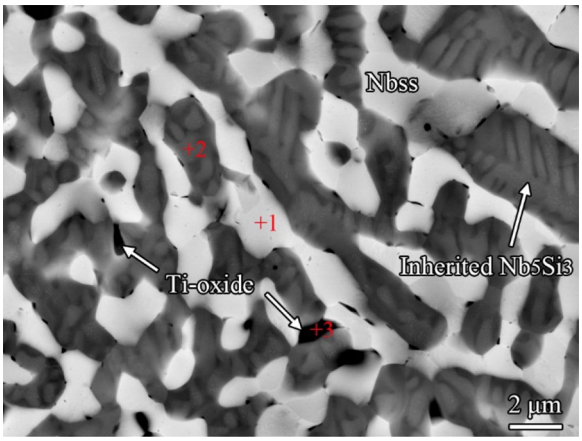

Figure 5 BSE image of the hypereutectic Nb-Si based alloy via EBSM after annealing treatment at 1450 °C for 5 h (+1, +2 and +3 are the positions for EDS measurements)

EBSD result in Figure 4(c), no specific crystal orientation relationship is found between β-Nb_5Si_3 and Nbss. Figure 4(d) displays the EDS mapping of a selected region in Figure 4(a), and it is noted that β-Nb_5Si_3 is enriched in Si, but depleted in Nb, Ti, Cr and Al relative to Nbss, which is identical to elemental distribution in the VIM alloy. Chemical segregations of Ti and Cr within both Nbss and Nb_5Si_3 phases are not found in the EBSM alloy.

To study the solid-state phase transformation of silicide dendrites formed via the rapid solidification process of EBSM, the annealing treatment has been performed at 1450 °C for 5 h, and the microstructure is shown in Figure 5. The compositions of selected positions in Figure 5, measured by SEM-EDS, is listed in Table 1. Combining this EDS result with XRD patterns in Figure 1, the dark-grey phase is determined to be Nb_5Si_3, including α- and β- forms, and the light-grey and dark phases are Nbss and Ti-oxide, respectively. The formation of Ti-oxide results from the high affinity of Ti for oxygen at elevated temperatures, and thus Ti atoms react with the residual oxygen during annealing treatment, particularly at grain boundaries and Nbss/Nb_5Si_3 phase interfaces [26]. The silicide dendrites after annealing treatment become coarsened second dendrite arm spacing increasing from ~0.9 μm to ~2.6 μm, and most of the nanoscale silicide particles no long exist, in comparison with the as-solidified microstructure in Figure 4(b).

Noteworthily, within the Nb_5Si_3 dendrites emerges a new dendritic silicide that shows a brighter BSE contrast, denoted as the inherited silicide in Figure 5, which, to our best knowledge, has not been reported previously. To reveal the crystal structure and identify the inherited silicide, STEM analysis has been performed, and the results are displayed in Figure 6. The SAD patterns of

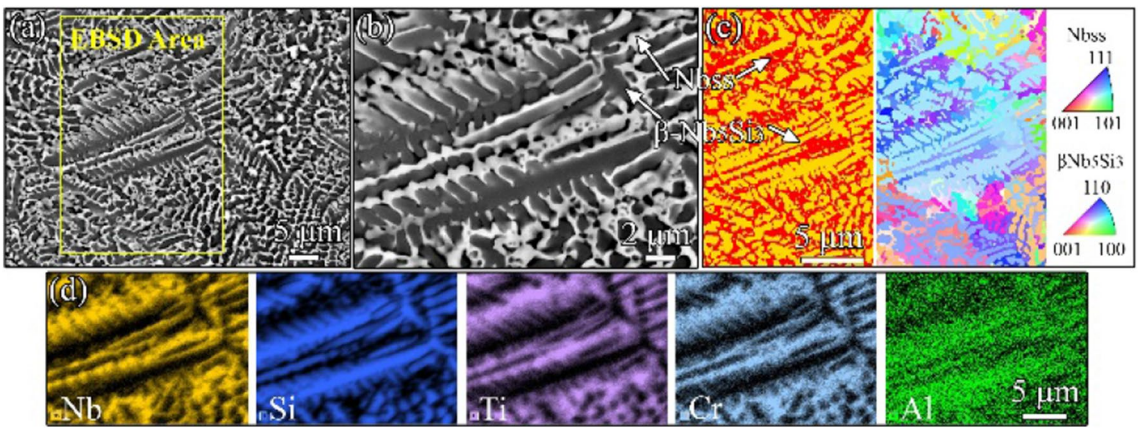

Figure 4 Microstructures and elemental distributions of the hypereutectic Nb-Si based alloy via EBSM: (**a**) BSE image; (**b**) Zoom-in BSE image; (**c**) EBSD phase and inverse pole figure (IPF) maps in the selected area in (**a**); (**d**) EDS mappings of (**b**)

Table 1 Compositions of selected positions in Figure 5 for the EBSM Nb-Si based alloy after annealing at 1450 °C for 5 h measured by SEM-EDS (at.%)

Position	O	Nb	Si	Ti	Cr	Al
+1	3.35	59.29	2.49	28.50	3.62	2.75
+2	1.77	43.90	31.93	20.49	0.19	1.72
+3	15.90	25.11	10.58	46.92	0.44	1.05

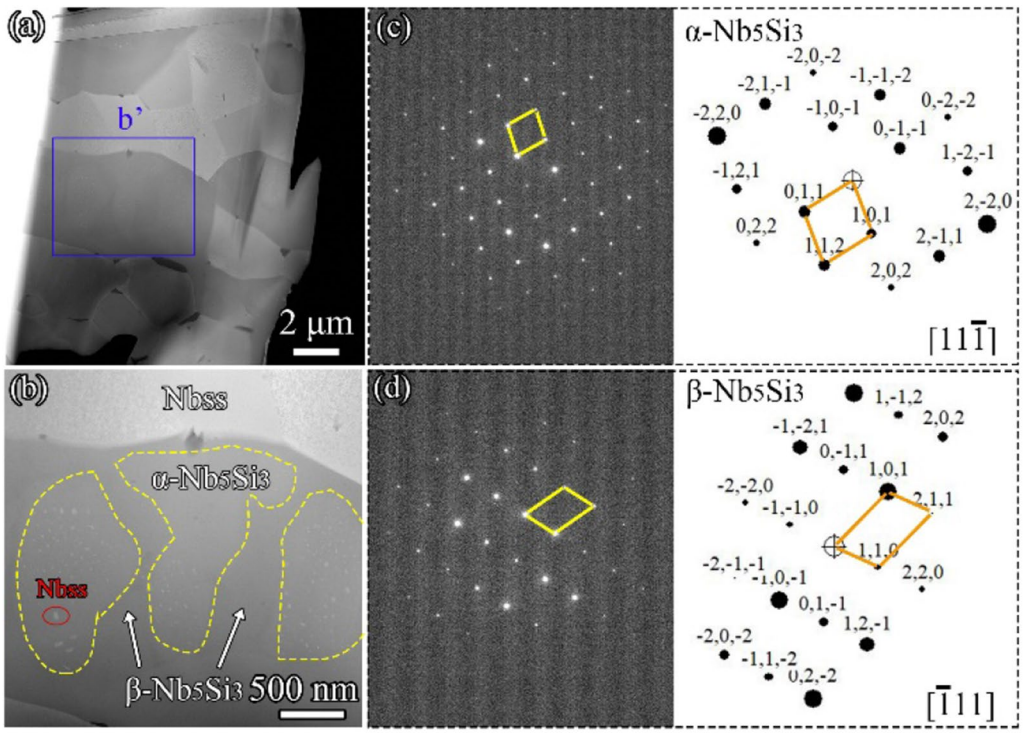

Figure 6 (**a**, **b**) HAADF-STEM images of the hypereutectic Nb-Si based alloy via EBSM after annealing treatment, (**c**) SAD patterns of α-Nb5Si3, (**d**) β-Nb5Si3

α-Nb5Si3[11-1] and β-Nb5Si3[-111] are obtained, which are in accordance with the simulated patterns using the CaRIne v3.1 software. Accordingly, it can thus be determined that the α-Nb_5Si_3 dendrites are formed within original β-Nb_5Si_3 dendrites, accompanied with the formation of Nbss particles (white contrast). This agrees with the result that both α-Nb_5Si_3 and β-Nb_5Si_3 are detected by XRD patterns (Figure 1). Such a phase transformation β-Nb_5Si_3→α-Nb_5Si_3 + Nbss has also been reported by Tsakiropoulos et al. [27, 28].

STEM-EDS has been further carried out to uncover the compositional difference between α-Nb_5Si_3 and β-Nb_5Si_3, as illustrated in Figure 7. Unfortunately, owing to the detecting limit of qualitative EDS approach, a well-defined compositional difference is not obtained. Even so, after careful checking, the inherited α-Nb_5Si_3 phase is slightly enriched in Nb and Al, and the β-Nb_5Si_3 phase shows the trace of higher Ti content. It is in accordance with observation that inherited α-Nb_5Si_3 displays a brighter Z-contrast than β-Nb_5Si_3 in the STEM-HAADF image (Figures 6(a) and 7(a)).

4 Discussion

Schematic of microstructure evolution the experimental Nb-Si based alloy under different solidification conditions of VIM and EBSM as well as subsequent annealing treatment is shown in Figure 8, with a particular focus on the morphology of intermetallic Nb_5Si_3 phases. The morphology change for Nb_5Si_3 found here is associated with its growth mode. For VIM processing with a near-equilibrium solidification condition, Nb_5Si_3 forms polyhedral morphologies, revealing a faceted solidifying

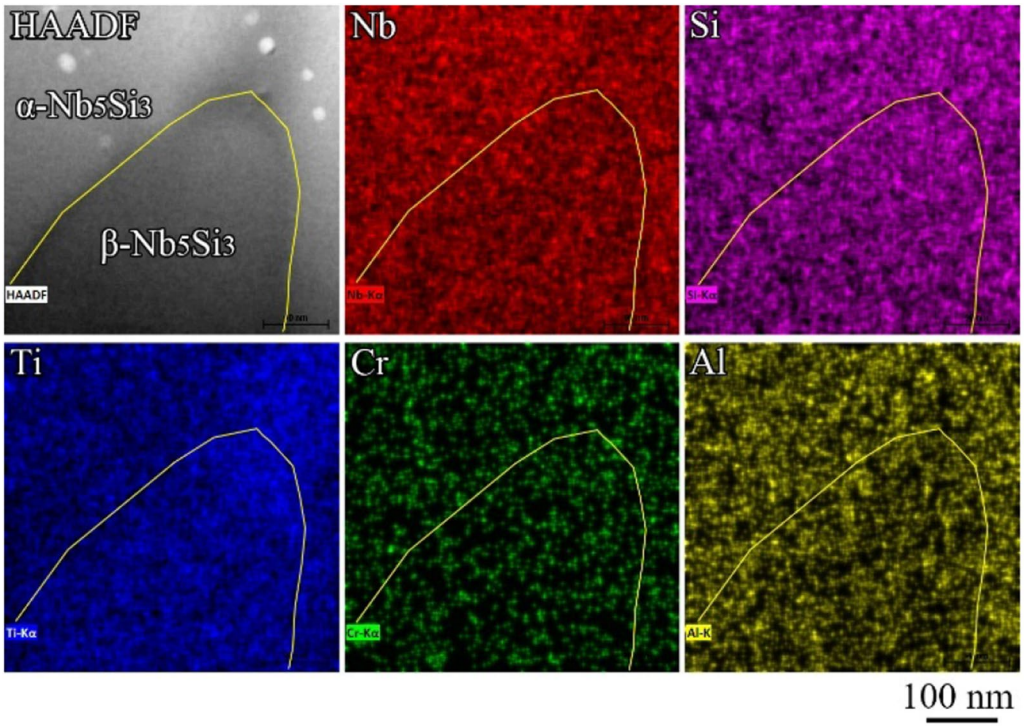

Figure 7 STEM-EDS mapping of the selected region for the hypereutectic Nb-Si based alloy via EBSM after annealing treatment at 1450 ℃ for 5 h, showing the distributions of Nb, Si, Ti, Cr and Al

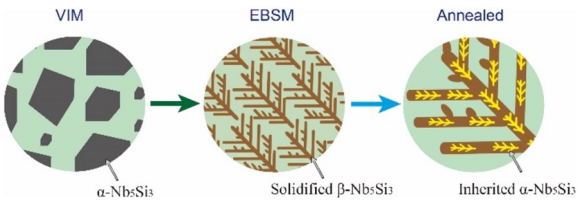

Figure 8 Schematic of morphology evolution of intermetallic Nb_5Si_3 phases in hypereutectic Nb-Si based alloys via VIM, EBSM and subsequent annealing treatment

mode. In terms of EBSM processing with a rapid solidification condition, Nb_5Si_3 dendrites are formed, displaying a non-faceted solidifying mode [14]. Namely, the transition from lateral growth (faceted) to continuous growth (non-faceted) is promoted by EBSM treatment.

The growth morphology of crystalline Nb_5Si_3 is normally determined by its intrinsic crystal structure and external solidification condition. The former dominates the equilibrium growth morphology via minimizing solid/liquid interface energy, and the latter indicated by undercooling can lead to the deviation from equilibrium morphology as determined by growth kinetics. During solidification, the solid/liquid interface, where attachment of atoms proceeds, shows a diffuse structure, and the interface roughness has been reported to determine the growth mode [29, 30]. With a relatively high entropy of fusion, Nb_5Si_3 crystal forms via the advancing of solid/liquid interface with evident growth anisotropy along different crystal orientations [10]. Under small undercooling of VIM processing, Nb_5Si_3 grows from atomically smooth solid/liquid interface in a lateral growth mode [10, 31]. Two dimensional nucleation on liquid/solid interface for Nb_5Si_3 is facilitated with the attachment of atoms rejected from the liquid to existing atomic steps on the growing interface [14, 32]. The atomic steps formed on liquid/solid interface are generally provided by the defects in Nb_5Si_3 crystal like dislocations. As a result, Nb_5Si_3 in the VIM alloy displays a faceted morphology (Figure 2).

For the rapid solidification process of EBSM, the undercooling significantly increases, and solid/liquid interface is suggested to become atomically roughened with the fraction of solid atom higher than 0.5 [15, 33]. Atoms tend to add to the interface without preferred crystal orientations, and the growth of Nb_5Si_3 crystal is in a continuous mode, instead of the lateral mode via two-dimensional nucleation. This can explain the direct formation of Nb_5Si_3 dendrites in EBSM alloy, which is an indication of continuous growth. Such microstructural transition from faceted to non-faceted growth enabled by a larger kinetic undercooling has been observed in the

solidification of some other materials with high entropy of fusion like primary Mg_2Si in Al-Mg_2Si alloys [15], silicon [34, 35], bismuth [17], germanium [36] and Al_2O_3 [37], etc.

It is interesting to find that the rapidly solidified β-Nb_5Si_3 phases can transform to the α-Nb_5Si_3 phases via annealing due to its better thermal stability at room temperatures, as indicated by the Nb-Si binary phase diagram [38]. The higher structural stability of α-Nb_5Si_3 has also been demonstrated by first principles calculations, in terms of cohesive energy and bonding electron number per atom [39]. Considering both α-Nb_5Si_3 and β-Nb_5Si_3 cells contain 20 niobium atoms and 12 silicon atoms [39], the precipitation of supersaturated Nb atoms in β-Nb_5Si_3, as a result of rapid solidification process of EBSM, happens together with the transformation from α-Nb_5Si_3 to β-Nb_5Si_3. It is worthy of note that the dendritic morphology remains (Figure 5). This may suggest such a phase transformation takes place in an in-situ way, rather than a nucleation precipitation process, which is associated with the short diffusion distance of atoms during annealing treatment [40]. As a result, a thermally stable hypereutectic Nb-Si based alloy, distinguished by a dendrite-dominated microstructure, is expected. The morphological evolution of primary Nb_5Si_3 found in this work can guide the artificial manipulation of the solidification processing with the aim of property optimization for Nb-Si based alloys, especially the fracture toughness at room temperature and the oxidation resistance at high temperatures.

5 Conclusions

Microstructures of the Nb-22Si-24Ti-2Cr-2Al (at.%) alloys prepared by VIM (near-equilibrium solidification) and EBSM (rapid solidification) techniques have been analyzed in this work, focusing on the Nb_5Si_3 growth response to solidification conditions. The following conclusions can be drawn from the experimental results.

(1) Tetragonal α-Nb_5Si_3 and β-Nb_5Si_3 phases are found in the experimental VIM and EBSM alloys. The decomposition of β-Nb_5Si_3 is facilitated by annealing at 1450 °C, resulting in α-Nb_5Si_3 formation.
(2) Primary Nb_5Si_3 dendrites are produced via a non-equilibrium solidification of EBSM, in contrast to the primary faceted Nb_5Si_3 particles in the VIM alloy. Significant microstructure refinement as well as a more homogeneous compositional distribution is achieved by EBSM, which is associated with its large solidification rate.
(3) The microstructure becomes coarser as a result of annealing. α-Nb_5Si_3 dendrites emerge within original as-solidified β-Nb_5Si_3 dendrites in the annealed alloys, with a slight enrichment of Nb and Al as well as a depletion of trace Ti.

Acknowledgements
The authors sincerely thanks to Dr. Hui Peng of Beihang University for his assistance on EBSM experiments.

Author Contributions
YG and LJ were in charge of the whole trial; YG wrote the manuscript; LJ and HZ provided conceptualization, investigation and manuscript review; WL assisted with sampling and laboratory analyses. All authors read and approved the final manuscript.

Authors' Information
Yueling Guo, born in 1990, is currently an associated research professor at *School of Mechanical Engineering, Beijing Institute of Technology, China*. His research interests include additive manufacturing and non-equilibrium solidification.
Lina Jia, born in 1981, is currently an associated professor at *Research Center of Light-alloy Materials, Frontier Institute of Science and Technology Innovation, Beihang University, China.*
Wenjun Lu, born in 1989, is currently a postdoctoral research fellow at *Max-Planck-Institut für Eisenforschung, Germany*. E-mail: luwj@sustech.edu.cn
Hu Zhang, born in 1968, is currently a professor at *Research Center of Light-alloy Materials, Frontier Institute of Science and Technology Innovation, Beihang University, China*.

Funding
Supported by National Natural Science Foundation of China (Grant No. 51571004).

Competing Interests
The authors declare no competing financial interests.

Author Details
[1]School of Mechanical Engineering, Beijing Institute of Technology, Beijing 100081, China. [2]Research Center of Light-alloy Materials, Frontier Institute of Science and Technology Innovation, Beihang University, Beijing 100191, China. [3]Max-Planck-Institut für Eisenforschung, Max-Planck-Straße 1, 40237 Düsseldorf, Germany.

Received: 29 January 2021 Revised: 1 June 2022 Accepted: 17 June 2022
Published online: 28 June 2022

References

[1] T M Pollock. Alloy design for aircraft engines. *Nature Materials*, 2016, 15(8): 809-815.
[2] J A Lemberg, R O Ritchie. Mo-Si-B alloys for ultrahigh-temperature structural applications. *Advanced Materials*, 2012, 24(26): 3445-3480.
[3] B P Bewlay, M R Jackson, P R Subramanian, et al. A review of very-high-temperature Nb-silicide-based composites. *Metallurgical and Materials Transactions A*, 2003, 34(10): 2043-2052.
[4] S Zhang, L Jia, Y Guo, et al. Improvement in the oxidation resistance of Nb-Si-Ti based alloys containing zirconium. *Corrosion Science*, 2020, 163: 108294.
[5] Y Qiao, X Guo, Y Zeng. Study of the effects of Zr addition on the microstructure and properties of Nb-Ti-Si based ultrahigh temperature alloys. *Intermetallics*, 2017, 88: 19-27.
[6] T Fei, Y Yu, C Zhou, et al. The deformation and fracture modes of fine and coarsened Nb_{SS} phase in a Nb-20Si-24Ti-2Al-2Cr alloy with a Nb_{SS}/Nb_5Si_3 microstructure. *Materials & Design*, 2017, 116: 92-98.
[7] S Yuan, L Jia, L Ma, et al. The microstructure optimizing of the Nb–14Si–22Ti–4Cr–2Al–2Hf alloy processed by directional solidification. *Materials Letters*, 2012, 84: 124-127.
[8] F Wang, L Luo, Y Xu, et al. Effects of alloying on the microstructures and mechanical property of Nb-Mo-Si based in situ composites. *Intermetallics*, 2017, 88: 6-13.

[9] B Jing, H Qiang, T Liang, et al. Liquid-solid phase equilibria of Nb-Si-Ti ternary alloys. *Chinese Journal of Aeronautics*, 2008, 21(3): 275-280.
[10] S V Meschel, O J Kleppa. Standard enthalpies of formation of some 4d transition metal silicides by high temperature direct synthesis calorimetry. *Journal of Alloys and Compounds*, 1998, 274(1): 193-200.
[11] W Liu, H Xiong, N Li, et al. Microstructure characteristics and mechanical properties of Nb-17Si-23Ti ternary alloys fabricated by in situ reaction laser melting deposition. *Acta Metallurgica Sinica (English Letters)*, 2018, 31(4): 362-370.
[12] Y Guo, Z Li, J He, et al. Surface microstructure modification of hypereutectic Nb-Si based alloys to improve oxidation resistance without damaging fracture toughness. *Materials Characterization*, 2020, 159: 110051.
[13] Y Guo, L Jia, B Kong, et al. Microstructure and surface oxides of rapidly solidified Nb-Si based alloy powders. *Materials & Design*, 2017, 120: 109-116.
[14] P C Bollada, P K Jimack, A M Mullis. Faceted and dendritic morphology change in alloy solidification. *Computational Materials Science*, 2018, 144: 76-84.
[15] C Li, Y Y Wu, H Li, et al. Morphological evolution and growth mechanism of primary Mg_2Si phase in Al–Mg_2Si alloys. *Acta Materialia*, 2011, 59(3): 1058-1067.
[16] J W Cahn, W B Hillig, G W Sears. The molecular mechanism of solidification. *Acta Metallurgica*, 1964, 12(12): 1421-1439.
[17] Z Jian, J Chen, F Chang, et al. Crystal-growth transition and homogenous nucleation undercooling of bismuth. *Metallurgical and Materials Transactions A*, 2011, 42(12): 3785.
[18] Y Guo, L Jia, B Kong, et al. Improvement in the oxidation resistance of Nb-Si based alloy by selective laser melting. *Corrosion Science*, 2017, 127: 260-269.
[19] Y Guo, J He, Z Li, et al. Tuning microstructures and improving oxidation resistance of Nb-Si based alloys via electron beam surface melting. *Corrosion Science*, 2020, 163: 108281.
[20] K Xu, Y Li, C Liu, et al. Advanced data collection and analysis in data-driven manufacturing process. *Chinese Journal of Mechanical Engineering*, 2020, 33: 43.
[21] C H Liebscher, V R Radmilović, U Dahmen, et al. A hierarchical microstructure due to chemical ordering in the bcc lattice: Early stages of formation in a ferritic Fe–Al–Cr–Ni–Ti alloy. *Acta Materialia*, 2015, 92: 220-232.
[22] I Papadimitriou, C Utton, P Tsakiropoulos. The impact of Ti and temperature on the stability of Nb_5Si_3 phases: a first-principles study. *Science and Technology of Advanced Materials*, 2017, 18(1): 467-479.
[23] M E Schlesinger, H Okamoto, A B Gokhale, et al. The Nb-Si (niobium-silicon) system. *Journal of Phase Equilibria*, 1993, 14(4): 502-509.
[24] J Xiong, Y Li, Z Yin, et al. Determination of surface roughness in wire and arc additive manufacturing based on laser vision sensing. *Chinese Journal of Mechanical Engineering*, 2018, 31: 74.
[25] J Huang, L Xue, J Huang, et al. Penetration estimation of GMA backing welding based on weld pool geometry parameters. *Chinese Journal of Mechanical Engineering*, 2019, 32: 55.
[26] S Mathieu, S Knittel, P Berthod, et al. On the oxidation mechanism of niobium-base in situ composites. *Corrosion Science*, 2012, 60: 181-192.
[27] C McCaughey, P Tsakiropoulos. Type of primary Nb_5Si_3 and precipitation of Nbss in αNb_5Si_3 in a Nb-8.3Ti-21.1Si-5.4Mo-4W-0.7Hf (at.%) near eutectic Nb-silicide-based alloy. *Materials*, 2018, 11(6): 967.
[28] K Zelenitsas, P Tsakiropoulos. Study of the role of Al and Cr additions in the microstructure of Nb–Ti–Si in situ composites. *Intermetallics*, 2005, 13(10): 1079-1095.
[29] T Riberi Béridot, M G Tsoutsouva, G Regula, et al. Strain building and correlation with grain nucleation during silicon growth. *Acta Materialia*, 2019, 177: 141-150.
[30] Y Chen, H M Wang. Growth morphologies and mechanism of TiC in the laser surface alloyed coating on the substrate of TiAl intermetallics. *Journal of Alloys and Compounds*, 2003, 351(1–2): 304-308.
[31] D Kang, T Zhang, C Jiang, et al. Preferred orientation transition mechanism of faceted-growth materials with FCC structure: Competitive advantage depends on 3D microstructure morphologies. *Journal of Alloys and Compounds*, 2018, 741: 14-20.
[32] H Kang, T Wang, Y Lu, et al. Controllable 3D morphology and growth mechanism of quasicrystalline phase in directionally solidified Al-Mn-Be alloy. *Journal of Materials Research*, 2014, 29(21): 2547-2555.
[33] R P Liu, W K Wang, D Li, et al. Transition from continuous to lateral growth for Ge crystal in undercooled $Ge_{74}Ni_{26}$ alloy melts. *Scripta Materialia*, 1999, 41(8): 855-860.
[34] Z Jian, K Nagashio, K Kuribayashi. Direct observation of the crystal-growth transition in undercooled silicon. *Metallurgical and Materials Transactions A*, 2002, 33(9): 2947-2953.
[35] R P Liu, T Volkmann, D M Herlach. Undercooling and solidification of Si by electromagnetic levitation. *Acta Materialia*, 2001, 49(3): 439-444.
[36] D Li, D M Herlach. Direct measurements of free crystal growth in deeply undercooled melts of semiconducting materials. *Physical Review Letters*, 1996, 77(9): 1801-1804.
[37] J A Sekhar, A Bharti, R Trivedi. Faceted-nonfaceted dendritic transitions during the laser processing of Al_2O_3-1.0 Wt Pct MgO. *Metallurgical Transactions A*, 1989, 20(10): 2191-2194.
[38] Y Li, W Zhu, Q Li, et al. Phase equilibria in the Nb–Ti side of the Nb–Si–Ti system at 1200 °C and its oxidation behavior. *Journal of Alloys and Compounds*, 2017, 704: 311-321.
[39] Y H Duan. Stability, Elastic constants and thermodynamic properties of (α, β, γ)-Nb_5Si_3 phases. *Rare Metal Materials and Engineering*, 2015, 44(1): 18-23.
[40] B Shao, Y Zong, D Wen, et al. Investigation of the phase transformations in $Ti_{22}Al_{25}Nb$ alloy. *Materials Characterization*, 2016, 114: 75-78.